EPJ Web of Conferences **334**, 04012 (2025) https://doi.org/10.1051/epjconf/202533404012
TGF'24

Self-Organization and Collective Dynamics of Cognitive Self-Steering Active Agents in Semi-Dense Systems

Priyanka IYER[1,*], *Rajendra Singh* NEGI[1,], *Andreas* SCHADSCHNEIDER[2,], and *Gerhard* GOMPPER[1,2,**]

[1]Theoretical Physics of Living Matter, Institute of Biological Information Processing and Institute for Advanced Simulation, Forschungszentrum Jülich, 52425 Jülich, Germany
[2]Institute for Theoretical Physics, Universität zu Köln, 50937 Köln, Germany

Abstract. The efficient movement of cognitive active agents, such as pedestrians, relies on adapting their motion in response to neighboring particles. We present a generic model for such systems, which consists of intelligent active Brownian particles (iABPs) in two spatial dimensions, moving at a constant speed along their heading direction. Essential features of this model are (i) steering torques that change the direction of motion related to visual perception for distancing and goal fixation, and (ii) a distinction between on-coming and co-moving agents. We examine semi-dense systems where excluded-volume interactions are negligible, and the constant-speed assumption applies. We use this model to describe two scenarios: motile agents at finite density, aiming to maintain a large neighbor distance, and agents at a three-way crossing, where there is no simple way to self-organize. In the first case, we find that the agent dynamics for medium-to-large vision angles only depend on the ratio $Pe^{3/2}/\Omega$ of their Péclet number Pe and maneuverability Ω, while for narrow vision angles, an avoidance-induced flocking state is observed. In the latter scenario, where agents aim to reach a goal, their behavior is governed by the competition of maneuverability, goal-fixation, the vision angle and the inflow rate.

1 Introduction

The collective motion of many particles or agents occurs in many living and engineered systems, over a wide range of length scales. On microscopic scales, bacteria and eukaryotic cells form biofilms and confluent monolayers, on macroscopic scales, ants, birds, sheep, and humans form flocks, trails, swarms, herds, and pedestrian crowds [1–3]. Generic features leading to collective motion in all these vastly different systems include (i) directional sensing of the position and orientation of neighboring particles, (ii) cognitive information processing and decision making about steering action or velocity adaptation, and (iii) collision avoidance to prevent damage or injury, as well as to avoid mutual blockage. In some systems, such as pedestrian crowds, each agent may also have a goal or target to achieve.

The observations of many systems mentioned above, such as bird flocks and semi-dense pedestrian crowds, indicate that self-steering, rather than speed adaptation governs agent behaviour [4–6]. Also, in most of these systems, inertia is not an important factor. Thus, it is

*e-mail: p.iyer@fz-juelich.de
**e-mail: g.gompper@fz-juelich.de

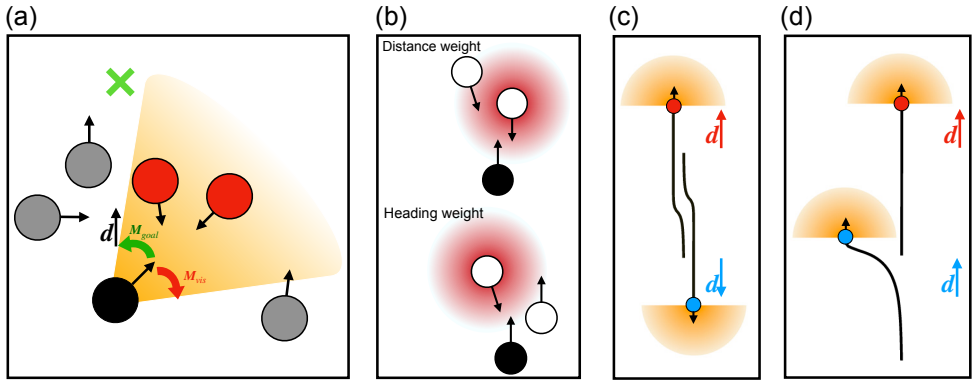

Figure 1. (a) Schematic showing the effect of the vision torque $\boldsymbol{M}_{vis}$ and goal-following torque $\boldsymbol{M}_{goal}$ on an agent (black). The vector $\boldsymbol{d}$ points towards the goal (green) and only the agents highlighted in 'red' are detected by the black particle. (b) Schematic showing the effect of the exponential and heading factors in T_{ij} [Eq.(5)], so that the highlighted (red) agents are avoided with larger weight/priority. Sample trajectories showing the effect of goal fixation and visual avoidance for (c) agents with opposite goal directions and (d) agents with the same goal direction. Here $\psi = \pi/2$, $\Omega = 1$, and $K = 1$. In (d) the red agent does not 'see' the blue one and therefore does not react.

a good approximation in modelling to assume a constant speed of all particles. Then, there are four possible types of steering requirements: (i) Short-distance avoidance by turning the direction of motion away from on-coming particles, (ii) trailing of co-moving particles ahead, or (iii) adjustment of the direction of motion to that of neighbors, and (iv) aiming for the group or swarm center for swarm cohesion [7–9]. Another important factor is of course the dimensionality of space, as motion of pedestrians through a quasi-one-dimensional narrow channel is certainly governed by other factors than the motion of a bird flock in three dimensions.

We focus here on the collective motion of agents in two spatial dimensions, applicable to pedestrians in a room [9], and at squares or crossings [10]. However, the model described below is very versatile, and can be easily adapted and generalized to other systems, including animal herds and bird flocks, as well as different environmental conditions such as navigation through channels and bottlenecks.

2 Model

We model pedestrians/agents as intelligent active Brownian particles (iABPs) in two spatial dimensions, moving at a constant speed v_0 along their heading direction $\mathbf{e}_i$. We employ a self-steering mechanism in the form of a torque that changes the direction of motion as

$$\dot{\mathbf{e}}_i = \sqrt{2(d-1)D_r}\boldsymbol{\Lambda}_i + \Omega\mathbf{M}_{\text{vis}} + K\mathbf{M}_{\text{goal}}, \tag{1}$$

where D_r is the rotational diffusion coefficient, d is the dimensionality, $\boldsymbol{\Lambda}_i$ is a Gaussian random process, Ω and K are the strength of the steering torques related to visual perception ($\mathbf{M}_{\text{vis}}$) and goal fixation ($\mathbf{M}_{\text{goal}}$), respectively. Agents steer towards their respective goals via the torque

$$M_{\text{goal}} = \left[\boldsymbol{e}_i \times \left(\hat{\boldsymbol{d}} \times \boldsymbol{e}_i\right)\right], \tag{2}$$

where the unit vector $\hat{\boldsymbol{d}}$ is the direction towards the goal, with which particle i attempts to align, see Fig. 1(a). Agents avoid collisions with each other via 'vision-assisted' reorientation

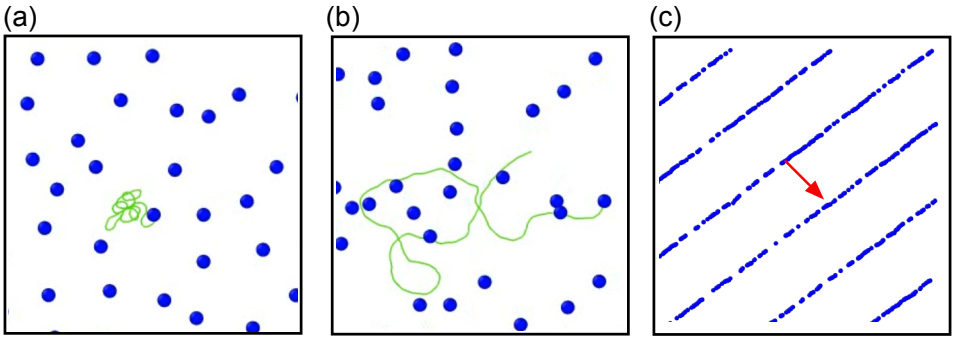

Figure 2. Trajectory (green) of a particle in the (a) overcautious regime ($Pe^{3/2}/\Omega = 0.0625$) and the (b) squirming regime ($Pe^{3/2}/\Omega = 0.5$) for density $\Phi = 0.25$ and vision angle $\psi = \pi/2$. (c) Avoidance induced flocking of particles at $\psi = \pi/4$, $Pe^{3/2}/\Omega = 0.125$, and $\Phi = 2.5$. The red arrow indicates the propagation direction of the particle. Adapted from Ref [9].

of their propulsion direction, which is described by the torque [10]

$$\mathbf{M}_{\text{vis}} = -\frac{1}{N_i}\sum_{j\in VC} T_{ij}\left[\boldsymbol{e}_i \times \left(\frac{\boldsymbol{r_{ij}}}{|\boldsymbol{r_{ij}}|}\times \boldsymbol{e}_i\right)\right], \tag{3}$$

where $\boldsymbol{r_{ij}} = \boldsymbol{r_j} - \boldsymbol{r_i}$ is the displacement vector between particle i and particle j. The sum is over all particles j that are in the vision cone VC of the agent i, with

$$VC = \left\{ j \mid \frac{\boldsymbol{r_{ij}}}{|\boldsymbol{r_{ij}}|}\cdot e_i \geq \cos\psi \text{ and } |\boldsymbol{r_{ij}}| < R_v \right\} \tag{4}$$

where ψ is the vision angle and R_v the vision interaction cutoff. T_{ij} is a weight factor given by

$$T_{ij} = e^{(-|\boldsymbol{r}_{ij}|/R_0)}[3 - \boldsymbol{e}_i \cdot \boldsymbol{e}_j]/4. \tag{5}$$

which increases the relative importance of avoiding agents moving 'head-on' towards each other ($\boldsymbol{e}_i \cdot \boldsymbol{e}_j = -1$), as opposed to co-moving agents (i.e. $\boldsymbol{e}_i \cdot \boldsymbol{e}_j = 1$) by a factor 1/2 [11]. The exponential distance dependence in Eq. (5) limits the range of the interaction, such that for high density of agents the effective vision range is R_0 and closer agents contribute more to the avoidance torque, see Fig. 1(b). Lastly, $N_i = \sum_{j\in VC} T_{ij}$ is the normalization factor, which makes the interactions non-additive. The activity of the agents is described by the Péclet number $\text{Pe} = v_0/R_0D_r$ and we measure K and Ω in units of D_r. By operating in the overdamped limit of the Langevin equation, we minimise the effects of inertia and the self-steering gives a realistic description of pedestrian movement. Figure 1(c,d) shows trajectories illustrating the combined effect of alignment and collision avoidance for agents with the same and opposite goal directions, where the former illustrates the non-reciprocity of the interactions.

3 Agents Maintaining Distances

We start by considering a simpler scenario where agents lack goal orientation, i.e. $K = 0$ and $\Omega > 0$, so that agents self-steer to avoid close encounters by moving away from locally sensed

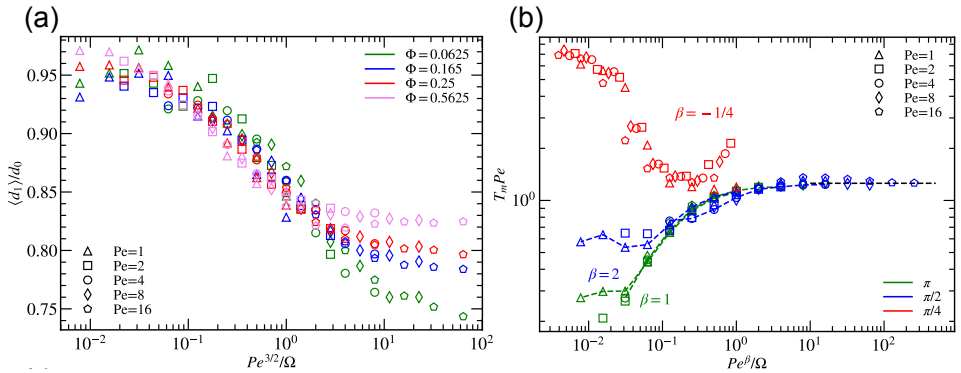

Figure 3. (a) Average nearest-neighbor distance $\langle d_1 \rangle$ for different pedestrian densities Φ as a function of $Pe^{3/2}/\Omega$. (b) Scaled average exposure time, $T_m Pe$ for different Péclet numbers Pe and $\Phi = 0.25$, with β ranging from $-1/4$ to 2 as indicated. Adapted from Ref [9].

regions of higher density. For simplicity, we also set $T_{ij} = \exp(-|\boldsymbol{r}_{ij}|/R_0)$, such that there is no perceived information on the heading direction of other agents, and only the distance weight contributes. N agents are placed in a box of size L with periodic boundary conditions, with the dimensionless particle density $\Phi = N(R_0/L)^2$. By using periodic boundary conditions, we isolate the effects of self-steering on agent dynamics and avoid wall-related effects like accumulation or rotating flows, which are not the focus of our study.

The behaviour of agents is found to depend only on the scaled variable $Pe^{3/2}/\Omega$. Specifically, we identify three distinct dynamic regimes: the overcautious regime, the squirming regime, and the reckless regime. In the overcautious regime ($Pe^{3/2}/\Omega \ll 1$), agents strongly avoid each other, resulting in minimal translational motion and a very low overall diffusion, see Fig. 2(a). In the squirming regime, vision-based steering enables agents to avoid collisions while maintaining some degree of translational motion [Fig. 2(b)]. Finally, in the reckless regime ($Pe^{3/2}/\Omega > 10$), agents exhibit high activity and move with little regard for their neighbors. Note that for all vision angles $\psi \geq \pi/2$, the long-time behavior of agents remains diffusive, due to the absence of a goal.

3.1 Nearest-Neighbour Distances and Exposure Time for Large Vision Angles

The analysis of the average nearest-neighbor distance $\langle d_1 \rangle$ and exposure time T_m provides insights into how effectively agents maintain a prescribed safety distance. Similar systems have been studied experimentally, particularly in the context of the COVID-19 pandemic [12]. We find that for vision angles $\psi \geq \pi/2$, agents come closer together as the density and/or activity is increased, consistent with experimental observations [12]. Moreover, the data collapses when expressed as a function of the scaled variable $Pe^{3/2}/\Omega$, see Fig. 3(a). A similar trend is observed for exposure time, which increases as agents transition from the overcautious to the reckless regime and is a universal function of the scaled variable Pe^{β}/Ω, where β depends on the vision angle [Fig. 3(b)].

3.2 Avoidance-Induced Flocking

For narrow vision angles (here $\psi = \pi/4$), we see an increase in the exposure time ($\beta < 0$, Fig. 3(b)) and a decrease in the average nearest-neighbor distance for low $Pe^{3/2}/\Omega$. Here, the

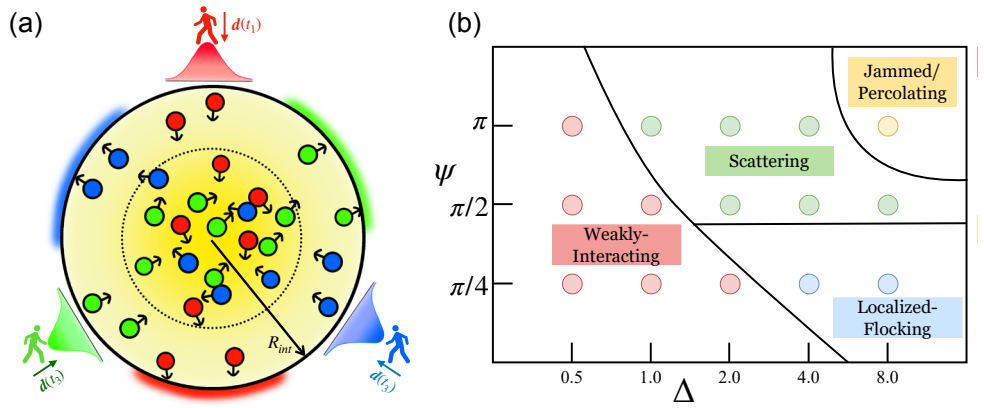

Figure 4. (a) Schematic of the three-way intersection, the three different pedestrian types are represented by the three colors with their respective goal directions $\boldsymbol{d}(t_i)$. The human markers show the position of influx placed on an interaction circle of radius $R_{\text{int}} = 120R_0$. (b) State diagram of pedestrian movement states as a function of the relative maneuverability$\Delta = \Omega/K$ and vision angle ψ. Here the dimensionless inflow rate $\Gamma = 1$. The lines serve as a visual guide to distinguish different dynamical 'states' and do not represent phase transitions in the statistical sense. Adapted from Ref [10].

combination of strong avoidance and a narrow vision angle leads to an avoidance-induced flocking state and band formations reminiscent of Viscek bands, as shown in Fig. 2(c). When the vision angle is small, the high perception asymmetry allows one agent to detect another while remaining undetected itself. The 'aware' agent initiates a turning motion to avoid a collision, however, as the unaware agent repeatedly re-enters its vision cone, the turning continues until both agents align and move in parallel, forming a co-moving cluster. This process repeats as additional agents align and integrate into the cluster, thus leading to an avoidance-induced flocking state.

4 Collective Behaviour of Agents at Intersections

We now consider agents chasing a goal ($K > 0$), initiating them at three equally spaced regions of a circle to create a basic realization of a three-stream intersection scenario [see Fig. 4(a)] [10]. The three-stream intersection scenario explored here is a basic realization of multi-directional pedestrian flow, as seen in busy intersections of malls, train stations, and large fairgrounds. Circle antipode experiments, in which participants are positioned on a circle and instructed to cross diagonally, explore a qualitatively similar setup [13, 14] and provide insights into navigation strategies at intersections. In our simulation, each agent tries to cross the interaction zone with the goal-following strength fixed at $K = 8$. We define the relative maneuverability $\Delta = \Omega/K$. Additionally, we now retain the heading factor in T_{ij} so that it has the form shown in Eq. (5). This has important consequences for the collective behaviour of the agents, as will be shown.

As the relative maneuverability Δ and the vision angle ψ are varied, the agents show different dynamical states, as shown in Fig. 4(b). For small $\Delta \lesssim 1$, agents head directly toward the goal, as goal alignment dominates over collision avoidance. As Δ is increased, pedestrian streams begin to interact and avoid each other, giving rise to complex motion patterns. Specifically, jammed, scattering, and localized flocking states emerge at vision angles $\psi = \pi$, $\psi = \pi/2$ and $\psi = \pi/4$ repectively.

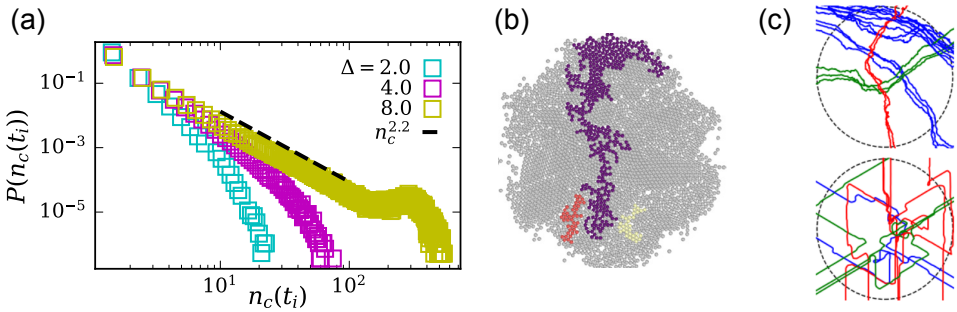

Figure 5. (a) Cluster size distribution of agents with the same goal direction shows the development of a power-law decay of the cluster size distribution as the system transitions from a free-flow to the jammed-percolated state for increasing Δ. (b) A snapshot highlighting the three largest clusters of same-type agents, demonstrating the percolated nature of clusters as they extend from the inflow to the exit. (c) Representative trajectories at $\Delta = 8$ for $\psi = \pi$ (top) and $\psi = \pi/4$ (bottom) highlighting features of fractional Brownian motion and Lévy-like walks, respectively. Adapted from Ref [10].

Percolated State: When the system enters a jammed state for large Δ, ψ, and Γ, the clustering behavior of agents changes significantly. Note that the jamming observed here is not caused by excluded volume effects but rather by strong steering avoidance and a large vision angle. By analyzing the cluster size distribution, we observe that the system transitions into a state where the clusters are percolated, i.e., clusters span the length of the interaction zone [Fig. 5(a,b)]. By self-organizing into percolated clusters, agents can navigate the crowded intersection and reach the exit. This is achieved by trailing agents with the same goal direction, thus bearing some similarities to lane formation seen in bi-directional flows. However, unlike stable lanes in bi-directional flows, these percolated clusters are transient, existing only for a single stream at a time and continuously breaking due to interactions with opposing streams.

Notably, the MSD of the agents increases in the jammed state compared to the scattering state, as following other agents results in more directed movement.

The analysis of the agents' dynamics for large Δ and ψ indicates that their motion can be effectively described by a fractional Brownian motion model (fBM) [for details see ref. [10]]. The trajectory for $\psi = \pi$ in Fig. 5(c) (top) shows that agents experience significant scattering, however, their overall movement is toward the goal. This can be characterized by positively correlated noise in the fBM model and leads to super-diffusive motion of the agents.

Localized Flocking: For narrow vision angles ψ and large local avoidance Δ, the agents in the interaction regime show avoidance-induced flocking, similar to the behavior observed in agents without goal following [Fig. 2(c)]. However, due to the presence of a goal, the global flocking state is disrupted, and only localized flocking emerges. Agents remain in these clusters until a combination of noise and goal-following disrupts this aligned state. In this regime, the motion of agents can be described as Lévy walks, due to longer flight states (i.e. flocking) followed by short reorientation events (collision avoidance), see Fig. 5(c).

5 Effect of Varying Inflow

In pedestrian, traffic, and even granular systems, the inflow rate of the constituents determines its state — whether it remains in free flow, becomes congested, or transitions into a jammed or clogged state [5]. The fundamental flow diagram measures the flux and average velocity of

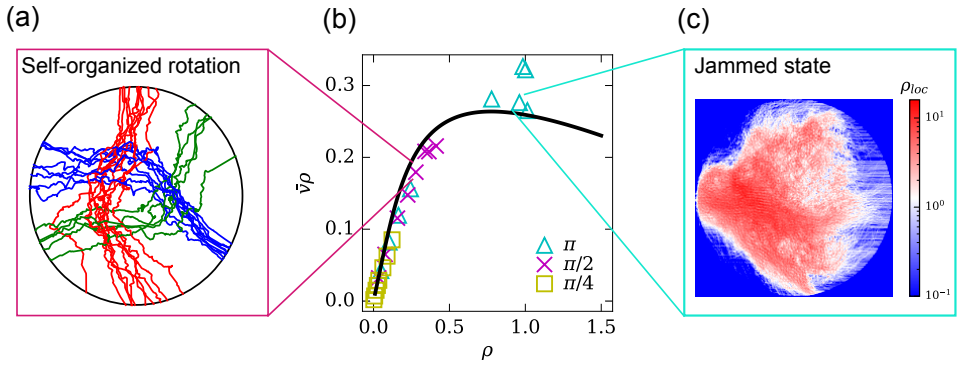

Figure 6. (a) Trajectories showing the self organisation into a rotational-state for $\Gamma = 2$, $\psi = \pi/2$, and $\Delta = 8$. (b) The fundamental flow diagram of the flux $v\rho$ as a function of ρ for the different vision angles shows a collapse of the data for the different vision angles. (c) The (single stream) local density ρ_{loc} heat-map shows the development of the jammed state, characterized by the reduced density at the exit and enhanced density at the inflow. Adapted from Ref [10].

agents/particles as a function of the density, which in-turn depends on the inflow. We focus on the regime of high avoidance (Δ) and vary the inflow rate Γ to investigate the resulting collective-behaviour of the system and construct the flow diagram. Notably, the data collapses onto a single master curve for different vision angles, see Fig. 6(b).

Depending on the vision angle and inflow rate, the system remains in different states of movement. For $\psi = \pi$, increasing Γ triggers a free flow to jamming transition, leading to a sudden rise in the average density and crowding at the entry [Fig. 6(c)]. In contrast, for $\psi = \pi/4$ the system always remains in the free-flow state as agents allow for closer proximity due to their narrow vision cones. For $\psi = \pi/2$, as the inflow increases, agents self-organize into a rotational state, as shown in Fig. 5(a). This self-organization is consistent with previous studies, which have demonstrated that pedestrian flows at intersections typically stabilize under rotational flow [15, 16]. The observed collective behaviours and agent dynamics, such as the percolated state, roundabout motion, and super-diffusive movement, emerge from the interplay between goal-following and the differential treatment of on-coming versus co-moving agents in collision avoidance.

6 Conclusions

We have shown how pedestrians can be modelled using intelligent active Brownian particles (iABPs) with self-steering torques for goal following and vision-based collision avoidance. In contrast to force-based models [17], we employ a local vision-based self-steering mechanism that adjusts the propulsion direction of agents through torques. Combining these steering-based interactions with the overdamped limit of the Langevin equation effectively mitigates artefacts arising from inertia effects seen in force-based models [18].

When only collision avoidance is considered, it is found that the agents display three movement states — overcautious, squirming, and reckless — depending on the scaled parameter $Pe^{3/2}/\Omega$. Similarly, the average nearest neighbour and exposure times are found to depend on the ratio between activity Pe and maneuverability Ω, with agents maintaining larger distances and minimizing exposure in the squirming and overcautious regimes. Notably, for narrow vision angles, avoidance-induced flocking emerges, leading to the formation

of band-like structures. When goal-following is considered, four classes of motion patterns are obtained for varying relative maneuverablity Δ and ψ — weakly interacting, locally flocking, strongly scattering, and jamming. The jammed state is found to show percolation, with the single agent dynamics well described by a fractional Brownian motion model with positively correlated noise. The fundamental flow diagram is found to be universal for different vision angles with agents displaying distinct collective behaviors as inflow increases, such as roundabout motion at $\psi = \pi/2$ and jamming at $\psi = \pi$.

Our results offer new insights into the dynamics of pedestrian and traffic systems, demonstrating how visual perception and goal-following can drive complex collective behaviors in congested environments. The close similarity of pedestrian motion to other "active matter" systems, such as cell suspensions, self-propelled colloids, and bird flocks, suggests that iABP models can serve as a unified framework for describing systems of cognitive active agents. Moreover, in contrast to the social force model, the iABP model features fewer parameters and non-additive interactions, making it more adaptable to complex scenarios—such as navigation in heterogeneous environments or modeling collective animal behavior with multiple interactions like alignment, collision avoidance, and trailing behavior.

References

[1] J. Elgeti, R.G. Winkler, G. Gompper, Physics of microswimmers—single particle motion and collective behavior: a review, Rep. Prog. Phys. **78**, 056601 (2015).

[2] G. Gompper, H.A. Stone, C. Kurzthaler, D. Saintillan, F. Peruani, D.A. Fedosov, T. Auth, C. Cottin-Bizonne, C. Ybert, E. Clément et al., The 2025 Motile Active Matter Roadmap, J. Phys. Condens. Matter (2025).

[3] A. Schadschneider, M. Chraibi, A. Seyfried, A. Tordeux, J. Zhang, Pedestrian dynamics: From empirical results to modeling, Crowd Dynamics, Volume 1: Theory, Models, and Safety Problems **1**, 63 (2018).

[4] E. Bosina, U. Weidmann, Estimating pedestrian speed using aggregated literature data, Phys. A: Stat. Mech. Appl. **468**, 1 (2017).

[5] A. Frohnwieser, R. Hopf, E. Oberzaucher, Human walking behavior–the effect of pedestrian flow and personal space invasions on walking speed and direction, Human Ethology **28**, 20 (2013).

[6] A. Cavagna, A. Culla, X. Feng, I. Giardina, T.S. Grigera, W. Kion-Crosby, S. Melillo, G. Pisegna, L. Postiglione, P. Villegas, Marginal speed confinement resolves the conflict between correlation and control in collective behaviour, Nat. Comm. **13**, 2315 (2022).

[7] S. Goh, R.G. Winkler, G. Gompper, Noisy pursuit and pattern formation of self-steering active particles, New J. Phys. **24**, 093039 (2022).

[8] R.S. Negi, R.G. Winkler, G. Gompper, Collective behavior of self-steering active particles with velocity alignment and visual perception, Phys. Rev. Res. **6**, 013118 (2024).

[9] R.S. Negi, P. Iyer, G. Gompper, Controlling inter-particle distances in crowds of motile, cognitive, active particles, Sci. Rep. **14**, 9443 (2024).

[10] P. Iyer, R.S. Negi, A. Schadschneider, G. Gompper, Directed motion of cognitive active agents in a crowded three-way intersection, Commun. Phys. **7**, 379 (2024).

[11] I. Karamouzas, B. Skinner, S.J. Guy, Universal power law governing pedestrian interactions, Phys. Rev. Lett. **113**, 238701 (2014).

[12] I. Echeverría-Huarte, A. Garcimartín, R. Hidalgo, C. Martín-Gómez, I. Zuriguel, Estimating density limits for walking pedestrians keeping a safe interpersonal distancing, Sci. Rep. **11**, 1534 (2021).

[13] Y. Xiao, Z. Gao, R. Jiang, X. Li, Y. Qu, Q. Huang, Investigation of pedestrian dynamics in circle antipode experiments: Analysis and model evaluation with macroscopic indexes, Transp. Res. Part C Emerg. **103**, 174 (2019).

[14] Y. Hu, J. Zhang, W. Song, Experimental study on the movement strategies of individuals in multidirectional flows, Physica A **534**, 122046 (2019).

[15] J. Ondřej, J. Pettré, A.H. Olivier, S. Donikian, A synthetic-vision based steering approach for crowd simulation, ACM Transactions on Graphics (TOG) **29**, 1 (2010).

[16] D. Helbing, P. Molnár, I.J. Farkas, K. Bolay, Self-organizing pedestrian movement, Environment and Planning B: Planning and Design **28**, 361 (2001).

[17] D. Helbing, P. Molnar, Social force model for pedestrian dynamics, Phys. Rev. E **51**, 4282 (1995).

[18] M. Chraibi, U. Kemloh, A. Schadschneider, A. Seyfried, Force-based models of pedestrian dynamics, Netw. Heterog. Media. **6**, 425 (2011).